



## Internal and tectonic evolution of Mercury

Steven A. Hauck, II<sup>a,b,\*</sup>, Andrew J. Dombard<sup>a,c</sup>, Roger J. Phillips<sup>c</sup>, Sean C. Solomon<sup>a</sup>

<sup>a</sup>Department of Terrestrial Magnetism, Carnegie Institution of Washington, Washington, DC, USA

<sup>b</sup>Department of Geological Sciences, Case Western Reserve University, Cleveland, OH, USA

<sup>c</sup>McDonnell Center for the Space Sciences and Department of Earth and Planetary Sciences, Washington University, Saint Louis, MO, USA

Received 17 October 2003; received in revised form 1 March 2004; accepted 24 March 2004

### Abstract

Mercury's geological and internal evolution presents an interesting enigma: are there conditions that allow for both apparently limited radial contraction over the last 4 billion years and sufficiently rapid core cooling at present to permit a hydromagnetic dynamo? To address this question, we simulate the coupled thermal, magmatic, and tectonic evolution of Mercury for a range of parameters (e.g., mantle rheology, internal heat production, core sulfur content) in order to outline the set of assumptions most consistent with these two conditions. We find that among the models tested, the only ones strictly consistent with  $\sim 1\text{--}2$  km of radial contraction since 4 Ga and a modern magnetic field generated by a core dynamo are those with a dry-olivine mantle rheology, heat production provided primarily by Th (negligible U or K), and a bulk core sulfur content  $>6.5$  wt%. However, because of the limited coverage and resolution of Mariner 10 imaging and derived topography, the tectonic history of an entire hemisphere is unknown. The potential for other mechanisms (e.g., long-wavelength lithospheric folds) to accommodate contraction remains untested, limiting the ability to restrict models on the basis of accumulated strain. Furthermore, Mercury's magnetic field may be a consequence of a thermoelectric dynamo or even crustal remanence; neither hypothesis places strong constraints on current heat flux from the core. Spacecraft observations of Mercury are needed to elucidate further the internal structure and evolution of the planet.

© 2004 Elsevier B.V. All rights reserved.

*Keywords:* Mercury; tectonics; internal evolution; mantle convection; magnetic field

### 1. Introduction

In the course of three flybys of Mercury in 1974–1975, Mariner 10 imaged  $\sim 45\%$  of the planet and revealed a generally ancient surface [1]. Mariner 10

images also showed distinctive tectonic features, termed lobate scarps. These structures are linear to arcuate in plan view, are tens to hundreds of kilometers in length, and have a maximum relief of hundreds of meters to a few kilometers [2,3]. Lobate scarps have been interpreted to be the surface expression of thrust faults formed as a result of global contraction [2,3]. The amount of shortening accommodated across lobate scarps on the imaged hemisphere of Mercury is consistent with globally averaged horizontal strains of  $\sim 0.05\text{--}0.1\%$ , equivalent to  $\sim 1\text{--}2$  km of radial

\* Corresponding author. Department of Geological Sciences, Case Western Reserve University, 112 A.W. Smith, 10900 Euclid Avenue, Cleveland, OH 44106-7216, USA. Tel.: +1-216-368-3675; fax: +1-216-368-3691.

E-mail address: [hauck@case.edu](mailto:hauck@case.edu) (S.A. Hauck, II).

contraction since the end of the period of heavy impact bombardment [2,3]. The most likely source of global contraction is net cooling of the planetary interior. Cooling leads to contraction through a reduction in average internal temperature and through internal phase changes (e.g., solidification). Differentiation of Mercury to form a molten, metallic core and silicate mantle and crust from an originally homogeneous state would have resulted in an increase in radius of  $\sim 17$  km and widespread evidence of surface extension [4]. Subsequent solidification of the core, if carried to completion, would result in a decrease in radius of  $\sim 17$  km and substantial contraction of the surface [4]. The absence of extensional features diagnostic of a global expansion (e.g., [5]) implies either that Mercury did not expand by such a large amount (e.g., because core segregation accompanied planetary accretion) or core formation must have substantially predated the end of heavy bombardment [4]. The limited contractional strain preserved in the lobate scarps may provide a constraint on the amount of global cooling and inner core solidification that has taken place since heavy bombardment. Whether this constraint provides a strict upper bound on global contraction, however, depends on whether strain has been accommodated by other mechanisms, such as faults unresolved in Mariner 10 images [2] or long-wavelength, low-amplitude folds [6].

The existence of Mercury's intrinsic magnetic field [7] also bears directly on the planet's internal evolution. Two hypotheses for the origin of the magnetic field are remanent magnetization (e.g., [8,9]) and an active core dynamo (e.g., [10]). Remanent magnetization has generally not been favored, for two reasons. Significantly greater specific magnetizations than typical on Earth are required; furthermore, the acquisition of coherent magnetization in a cooling lithosphere requires that a single polarity for the internal dipole field persisted over a time scale substantially longer than the characteristic interval between polarity reversals on Earth [11]. Observations of high crustal remanent magnetizations on Mars [12], however, warrant a reexamination of this hypothesis for Mercury [13].

A dynamo origin for Mercury's magnetic field would place an important additional constraint on the present internal structure and thermal state of the planet. Magnetic field generation via dynamo action requires that some fraction of the core be molten and

that there be an energy source for convective motions within the liquid layer (e.g., [14]). Calculations indicate that a core composed solely of iron or iron and nickel should be completely solid at present (e.g., [4]), precluding a core dynamo; however, complete core solidification would result in up to 15 times more radial contraction than has been inferred from surface tectonics [4]. A light alloying element, such as sulfur (e.g., [15]), may reduce the melting point of the core to the point where a liquid outer core persists to the present [4,11,16,17].

In the time since the Mariner 10 mission, our understanding of important aspects of planetary evolution, including mantle convection (e.g., [18,19]), the behavior of core-forming materials at high temperatures and pressures (e.g., [20,21]), and magnetic field generation (e.g., [14]), has progressed significantly. Thirty years after the first flyby of Mercury by Mariner 10 (e.g., [5]), NASA's MESSENGER spacecraft [22] is scheduled for launch in 2004 and will be followed by the BepiColombo mission of the European Space Agency and the Japanese Institute of Space and Astronautical Science (e.g., [23]) early in the following decade. Our goal here is to sharpen our understanding of Mercury's internal evolution in anticipation of results from these forthcoming missions. We model the thermal and tectonic evolution of Mercury in order to explore the effects of variations in initial conditions and internal material properties on accumulated surface strain and the potential for convection in the outer core.

## 2. Modeling

Our approach to modeling the internal evolution of Mercury is to calculate both the convective and conductive parts of the planet's heat loss through time. We accomplish this modeling via a parameterized mantle convection technique (e.g., [11,17,24]) modified to include the potential transition to a fully conductive mode of heat transfer; see [24] for a complete description of the model. Model parameters and their nominal values are listed in Table 1. We assume that core differentiation proceeded early in the planet's history by analogy with Mars [25], where the  $^{182}\text{Hf}$ – $^{182}\text{W}$  isotope systematics suggest that separation of metal from silicate materials was complete

Table 1  
Summary of model parameters

| Parameter   | Symbol       | Value                       | Units               |
|---|--------------|-----------------------------|---------------------|
| Normalized moment of inertia                          | $C/MR_p^2$   | 0.33                        | –                   |
| Radius of planet                                      | $R_p$        | $2440 \times 10^3$          | m                   |
| Radius of core  | $R_c$        | 1803–<br>$1868 \times 10^3$ | m                   |
| Density of mantle                                     | $\rho_m$     | 3400                        | kg/m <sup>3</sup>   |
| Heat capacity of mantle                               | $c_m$        | 1212                        | J/(kg K)            |
| Density of core                                       | $\rho_c$     | 7200                        | kg/m <sup>3</sup>   |
| Heat capacity of core                                 | $c_c$        | 465                         | J/(kg K)            |
| Core sulfur mass fraction                             | $\chi_s$     | 0.0–0.1                     | –                   |
| Surface temperature                                   | $T_s$        | 440                         | K                   |
| Initial upper mantle temperature                      | $T_{u0}$     | 1800–2100                   | K                   |
| Initial CMB temperature                               | $T_{c0}$     | 1925–2225                   | K                   |
| Surface gravitational acceleration                    | $g$          | 3.7                         | m/s <sup>2</sup>    |
| Volumetric coefficient of thermal expansion           | $\alpha_v$   | $3 \times 10^{-5}$          | K <sup>-1</sup>     |
| Mantle thermal diffusivity                            | $\kappa$     | $1 \times 10^{-6}$          | m <sup>2</sup> /s   |
| Mantle thermal conductivity                           | $k$          | 4                           | W/(m K)             |
| Ductile creep viscosity constant                      | $A^*$        | $3.5 \times 10^{22}$        | 1/s                 |
| Rigidity of mantle                                    | $\mu$        | $80 \times 10^9$            | Pa                  |
| Ductile creep stress exponent                         | $n$          | 3.5                         | –                   |
| Ductile creep activation energy                       | $E_a$        | $540 \times 10^3$           | J/mol               |
| Ductile creep activation volume                       | $V$          | $15–25 \times 10^{-6}$      | m <sup>3</sup> /mol |
| Solid–liquid distribution coefficient                 | $D$          | 0.1                         | –                   |
| Mantle heat of fusion                                 | $L_{pm}$     | $600 \times 10^3$           | J/kg                |
| Core heat of fusion                                   | $L$          | $250 \times 10^3$           | J/kg                |
| Inner core gravitational energy release               | $E_g$        | $250 \times 10^3$           | J/kg                |
| Iron melting temperature (STP)                        | $T_{m0}$     | 1809                        | K                   |
| Melting curve coefficient                             | $T_{m1}$     | $1.54 \times 10^{-11}$      | Pa <sup>-1</sup>    |
| Melting curve coefficient                             | $T_{m2}$     | $-1.17 \times 10^{-22}$     | Pa <sup>-2</sup>    |
| Core adiabat coefficient                              | $T_{a1}$     | $8 \times 10^{-12}$         | Pa <sup>-1</sup>    |
| Core adiabat coefficient                              | $T_{a2}$     | $-3.9 \times 10^{-23}$      | Pa <sup>-2</sup>    |
| Initial crustal thickness                             | $d_{c0}$     | 0                           | m                   |
| Mantle compressibility                                | $\beta_m$    | $3 \times 10^{-12}$         | Pa <sup>-1</sup>    |
| Outer core compressibility                            | $\beta_{oc}$ | $2 \times 10^{-11}$         | Pa <sup>-1</sup>    |
| Inner core compressibility                            | $\beta_{ic}$ | $3 \times 10^{-12}$         | Pa <sup>-1</sup>    |
| Young's modulus of the lithosphere                    | $E$          | $1 \times 10^{11}$          | Pa                  |
| Poisson's ratio of the lithosphere                    | $\nu$        | 0.25                        | –                   |
| Fractional liquid–solid volume change in $\gamma$ -Fe | $\zeta$      | 0.05                        | –                   |
| Elastic blocking temperature                          | $T_b$        | 950                         | K                   |
| Strain accumulation start-time                        | $t_e$        | 4.0                         | Ga                  |

within 15 My of the start of solar system formation. This assumption of early core separation is in accord with the lack of evidence for the widespread surface extension that would accompany late planetary differentiation (e.g., [4,5]). Core cooling and inner core growth are significant contributors to the internal evolution of a planet, particularly one with a relatively large core. We account for the effects of a cooling core, the latent heat of freezing, and gravitational energy released as heat during inner core growth following Eqs. (3)–(7) of Stevenson et al. [17], but the melting relations for a presumed Fe–FeS core have been updated with recent experimental results [21,26]. In this model for core evolution, the inner core size is determined by finding the intersection of the core melting curve and the adiabat subject to the condition of mass balance of light element and to the assumption that the inner core is pure Fe. The  $\gamma$ -Fe phase [27] is expected under conditions anticipated within the core of Mercury and we adopt values for physical parameters on this basis. In all model cases, the moment of inertia,  $C$ , is taken to satisfy  $C/MR_p^2 = 0.33$ , where  $M$  and  $R_p$  are the mass and radius of the planet respectively, a value suggested by recent models for Mercury's internal structure [28] to be consistent with a range of core sulfur contents from 0 to 10 wt%. An important aspect of the thermal evolution of a planet is partial melting of the mantle, which we include by coupling a model for batch partial melting [29] of peridotite [30] to the parameterized convection model by including explicitly the fractionation of heat-producing elements and the latent heat of melting of mantle materials [24].

We employ a one-dimensional representation of convective heat transfer in a spherical shell overlying a spherical core. Convection in the mantle is parameterized via a relationship between the vigor of convection (described by the Rayleigh number,  $Ra$ , the ratio of buoyancy to viscous forces) and the efficiency of convective heat transfer (defined by the Nusselt number,  $Nu$ , the ratio of total heat flux to the conducted heat flux) (e.g., [19]). We use  $Nu = (0.31 + 0.22n)\theta^{(-2(n+1)/(n+2))} Ra^{(n/(n+2))}$  [18], where  $n$  is the exponent of the deviatoric stress in the flow law (e.g.,  $n=1$  for Newtonian fluids), and  $\theta$  is the natural logarithm of the contrast in viscosity across the layer. Using the  $Ra$ – $Nu$  relationship as a constraint, the thermal evolution models are calculated by solving

the equation for the conservation of energy as a function of time for a convecting mantle with internal heating, a cooling (and possibly solidifying) core, and a thickening (or thinning) lithosphere with a crust.

Our implementation differs from the typical approach (e.g., [11,17]) in two major ways. First, we explicitly solve the nonlinear, time-dependent, heat conduction equation in the thermal lithosphere by means of a finite element solution with adaptive remeshing [24]. Second, without explicitly modeling the melt transport process, we include the energetics of partial melting in the mantle energy balance through the latent heat of melting, which acts as an energy sink in the mantle and an energy source in the crust. We also utilize scaling laws derived from numerical models of convection in fluids with strongly temperature- and pressure-dependent viscosity (e.g., [18,31–33]) rather than the isoviscous  $Ra-Nu$  scaling relationships employed in earlier studies of Mercury's internal evolution (e.g., [11,17]). Temperature-dependent viscosity models, in contrast to uniform-viscosity models, tend to develop thick, stagnant lids that are analogous to the lithospheric shell on one-plate planets. The Rayleigh number of Mercury's comparatively thin mantle is substantially smaller than those for the other inner planets [ $Ra \sim (R_p - R_c)^\beta$  where  $R_c$  is the radius of the core and  $\beta$  is a constant, e.g.,  $\beta = 3$  for bottom-heated Newtonian fluids]. Furthermore, increasing pressure tends to suppress the vigor of mantle convection through an increase in the effective viscosity relative to a nonpressure-sensitive system (e.g., [32]), which can be important in a planet where the Rayleigh number is modest. For these reasons, some fraction of Mercury's evolution may have operated in a conductive rather than convective mode of mantle heat transport. We extend our finite element scheme for the lithosphere to the mantle in order to calculate the thermal history of the mantle during such time intervals.

Some understanding of a planet's bulk composition and mineralogy is crucial for models of its internal evolution, yet for Mercury these parameters are poorly constrained (e.g., [34]). Despite this uncertainty, we can place bounds on thermal models by investigating the consequences of a range of parameter choices. The concentrations of long-lived heat-producing elements such as potassium, uranium, and thorium control a primary source of heat within the

planet. Mercury's concentrations of these elements are unknown, but compositional models [35] range from a condensation-sequence-dominated assemblage with amounts of U and Th similar to the Earth's upper mantle and negligible K [36] to a Th-rich and U- and K-poor model under conditions of late-stage silicate vaporization [37]. Potassium has been detected in Mercury's exosphere (e.g., [38]) and is inferred to be a surface component, albeit of unknown concentration. A third model of Mercury's bulk composition centers around the possibility that the planet's large bulk density of  $5430 \text{ kg/m}^3$  is the result of one or more giant impacts having stripped off most of the outer, silicate-rich layers of a larger protoplanet (e.g., [39]). A formational history of this type could have left behind a mantle composition similar to that of CI chondrites (e.g., [35]). Given the different compositions of heat-producing elements predicted by these models, our aim is to assess whether current hypotheses for Mercury's formation are consistent with the potential constraints on the planet's internal evolution.

Mantle viscosity is strongly dependent on temperature, pressure, mineralogy, and water content. We assume, on the basis of analogy with the Earth's mantle, that the mantle mineralogic assemblage is dominated by olivine, for which there has been considerable experimental work on the dependence of viscosity on these parameters (e.g., [40]). The melting behavior of mantle materials is also strongly dependent on composition and mineralogy. In order to assess the potential importance of mantle melting on Mercury's internal evolution, we employ melting relationships for a mantle assemblage represented by KLB-1 peridotite [30]. This approach is consistent with the olivine-rich mineralogy assumed for the mantle viscosity and applicable to Mercury because although the iron content of Mercury's mantle plus crust may be quite low relative to that of the Earth (e.g., [41,42]), the iron content of peridotite does not significantly perturb the solidus [43,44]. In model cases with mantle melting, heat-producing elements are fractionated with a solid-liquid partition coefficient of 0.1, and the melt is added to the crust, where heat production is assumed to decrease exponentially with depth (e.g., [24]) consistent with the upward concentration of incompatible elements during melting and crustal formation.

To model the surface strain history, we assume that the lithosphere may be represented as an elastic shell overlying an inviscid mantle and core. Coupled to the thermal solution, we calculate the accumulated strain in the elastic lithosphere for comparison with the estimated strain accommodated by lobate scarps. Details of the strain calculations are given in Appendix A. Strain accommodated within the elastic shell is derived from volumetric changes resulting from the cooling of the lithosphere, mantle, and core, as well liquid–solid phase changes. The finite thickness of the elastic lithosphere is defined by the depth to an elastic blocking temperature,  $T_b$  [45]. The value of  $T_b$  may be bounded by analogy with terrestrial oceanic lithosphere, for which flexural models indicate an inability to support elastic stress differences at temperatures as low as  $\sim 800$  K [46] and the base of the seismogenic zone, which is approximately coincident with an isotherm as high as  $\sim 1100$  K [47]. We adopt a nominal value for  $T_b$  of 950 K.

### 3. Results

We explore the effects that core sulfur content, magmatism, mantle rheology, initial thermal state, internal heat production, and pressure dependence of core melting relations have on the tectonic evolution of the surface and on the prospects for a core dynamo to generate a modern magnetic field. We begin with an illustrative model case for Mercury's thermal evolution to highlight the basic features of the planet's evolution. For this and later model cases, we focus on two parameters. The first is the ratio of the present inner core radius to outer core radius ( $R_i/R_c$ ) because of the direct influence that inner core growth has on both planetary contraction and magnetic field generation. The second is the time-integrated surface strain since 4 Ga. Because of the strong melting-point depression with increasing sulfur content (up to the eutectic composition) for core materials, our results for inner core size and surface strain are compared as a function of bulk core sulfur content.

#### 3.1. Example thermal evolution model case

The illustrative model case has a bulk core sulfur content of 8.5 wt% and an initial temperature at the

base of the lithosphere of 1800 K (see Table 1 for other parameter values). In all model cases (except where otherwise noted), the initial temperature difference between the upper mantle and core–mantle boundary (CMB) is 125 K, yielding an approximately adiabatic gradient in the mantle. The core temperature distribution is also taken to be adiabatic. Heat production follows from assumed abundances of U and Th, but with no K, consistent with a condensation-sequence-dominated (Table 2) planetary composition [36].

The evolution of mantle and CMB temperatures (Fig. 1a) displays a rapid decrease in temperature from the initial state followed by more moderate cooling paralleling the decay in the concentration of heat-producing elements. The large initial drop in mantle temperature is due to the extraction of a substantial amount of partial melt from the mantle. Mantle convection ceases at  $\sim 3.3$  Ga, after which CMB temperatures indicate a readjustment in the rate of heat loss due to the change in dominant mechanism of heat transport. An inflection at  $\sim 0.8$  Ga is due to the energy released on first appearance of a solid inner core. The history of heat flux (Fig. 1b) is similar to that for mantle temperature, yet it also illustrates the contribution of crustal heat production to early surface heat flow. Upon cessation of mantle convection core, heat flux first becomes negative then grows increasingly positive due to a transient increase in lower mantle temperature as the mantle adjusts to the lack of convection and cooling of the core and mantle and recurs following the adjustment period. The inner core grows to 20% of the outer core radius by the present (Fig. 1c). The crust forms early (Fig. 1d), the consequence of an early demise of a region of pervasive partial melting that extends from the base of the

Table 2  
Adopted models for the abundances of heat-producing elements in the silicate fraction of mercury

| Model            | U<br>(ppb) | Th<br>(ppb) | K<br>(ppm) |
|------------------|------------|-------------|------------|
| Condensation     | 30         | 120         | 0          |
| Vaporization     | 0          | 400         | 0          |
| Condensation + K | 30         | 120         | 100        |
| CI chondrite     | 8          | 30          | 550        |
| 1/2 CI chondrite | 4          | 15          | 275        |

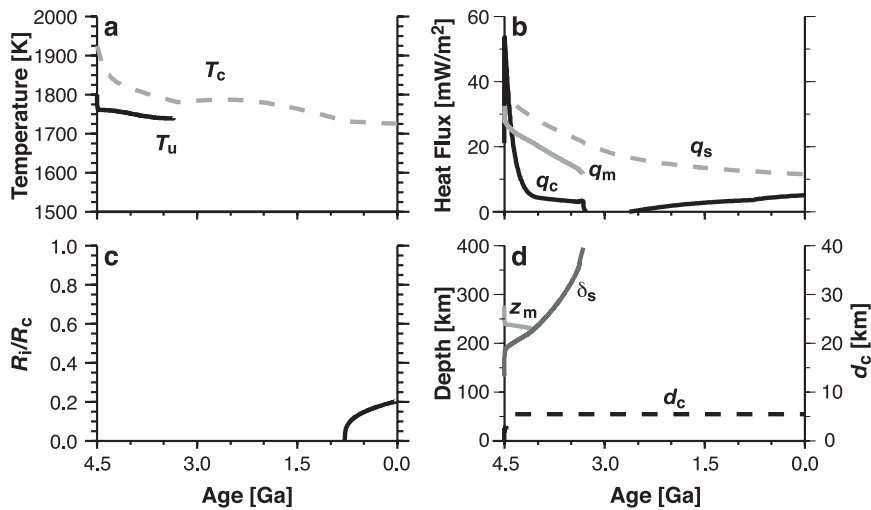


Fig. 1. Illustrative thermal evolution scenario with 8.5 wt% S in the core; silicate heat production given by U and Th abundances for a condensation-sequence-dominated composition; a non-Newtonian, pressure-dependent mantle rheology appropriate for dry olivine; partial melting of the mantle and melt transport to the crust; and an initial upper mantle temperature of 1800 K. (a) Temperatures  $T_c$  and  $T_u$  at the core–mantle boundary and the base of the thermal lithosphere, respectively. (b) Heat flux at the surface,  $q_s$ , base of the lithosphere,  $q_m$ , and core–mantle boundary,  $q_c$ . (c) Ratio of inner core radius to outer core radius. (d) Greatest depth of pervasive partial melting,  $z_m$ , lithospheric thickness,  $\delta_s$ , and crustal thickness,  $d_c$ .

lithosphere ( $\delta_s$ ) to the maximum depth of partial melting ( $z_m$ ) as the lithosphere thickens.

### 3.2. Effect of melt extraction

The formation of crust enriched in incompatible heat-producing elements by the transport of partial melt from the mantle can influence planetary thermal evolution, particularly early cooling (e.g., [24]). Early cooling, in turn, may influence the post-4-Ga rate of cooling potentially responsible for Mercury's global system of contractional faults. The effect of crustal growth is visible in Fig. 2, which compares suites of models with and without melting. The rapid, early cooling (prior to the end of heavy bombardment, when the strain calculation begins) of the interior that accompanies magmatic extraction of heat generally reduces the integrated global contraction and surface strain subsequent to 4 Ga, particularly at low core sulfur contents (<5 wt%). Another result of the enhanced cooling accompanying mantle melt extraction is a relatively larger inner core at present, an effect most noticeable at high core sulfur contents.

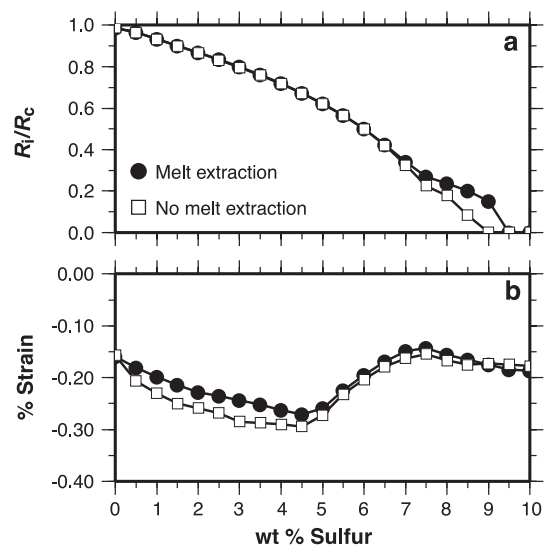


Fig. 2. Comparison of the effects of mantle melt production and crustal growth on (a) the present normalized inner core radius and (b) surface strain accumulated over the last 4 Gy as functions of bulk core sulfur content for a dry-olivine mantle rheology, condensation-sequence-dominated U and Th, and an initial upper mantle temperature of 1800 K.

The maximum contractional strain (negative by convention), with or without melt extraction, occurs at  $\sim 4\text{--}5$  wt% S, for reasons discussed in Section 3.4.

### 3.3. Effect of mantle rheology

Efficient transport of heat by the mantle is limited by the rate at which mantle materials can flow. Our models include a non-Newtonian, temperature- and pressure-dependent mantle viscosity appropriate for olivine. A substantial uncertainty in rheological parameters for the non-Newtonian creep behavior of olivine is the activation volume, because the range of current estimates varies more than 50% from nominal values [40]. This range in activation volume translates into an uncertainty in inner core radius of up to 20% at high core sulfur contents (Fig. 3a) and an uncertainty of 0.05–0.1% in accumulated surface strain (Fig. 3b).

Water substantially reduces the viscous strength of mantle materials (e.g., [40,48,49]), leading to more efficient convective heat transport. This lowered mantle viscosity results in a larger inner core and more contraction relative to scenarios with an anhydrous mantle (Fig. 4). None of the wet-olivine cases have a

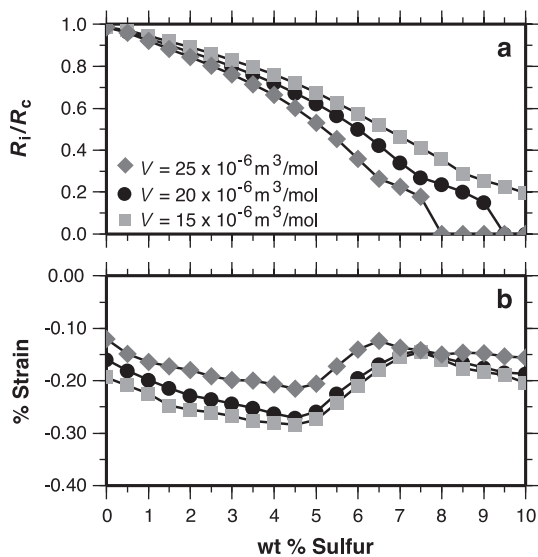


Fig. 3. Comparison of the effects of variations in the activation volume for mantle creep on (a) normalized inner core radius and (b) accumulated surface strain as functions of bulk core sulfur content for a dry-olivine mantle rheology, condensation-sequence-dominated U and Th, mantle melt production and crustal growth, and an initial upper mantle temperature of 1800 K.

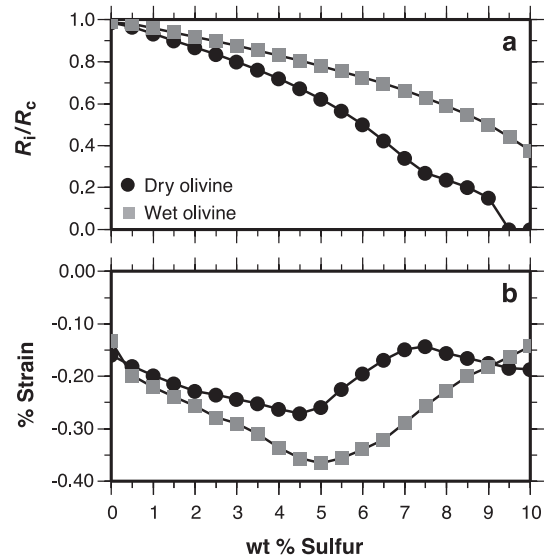


Fig. 4. Comparison of the effects of wet-olivine vs. dry-olivine mantle rheology on (a) normalized inner core radius and (b) accumulated surface strain as functions of bulk core sulfur content for condensation-sequence-dominated U and Th and an initial upper mantle temperature of 1800 K.

$R_i/R_c$  values at present smaller than 0.35. Cases with a wet-olivine rheology predict up to 0.15% more contractional strain than the dry models, a difference greater than the upper bound on contractional strain of  $\sim 0.1\%$  inferred from lobate scarps [2]. A notable exception is the set of models with a wet-olivine mantle rheology and more than  $\sim 9$  wt% bulk core sulfur, which predict less integrated contractional strain than the dry-olivine models, aided in large part by the substantial latent heat and gravitational energy released over time by inner core growth.

### 3.4. Effect of initial thermal state

The early thermal state of a planetary interior affects both the initial physical structure (e.g., solid fraction of the core) and the efficiency of early heat transport. The effect of different initial internal temperature profiles is shown in Fig. 5, for scenarios with (open symbols) and without (closed symbols) extraction of melt. Initial temperatures, over the range shown, have a small effect on the present inner core radius. The same is true for integrated surface strain for core sulfur contents greater than  $\sim 6$  wt%. At

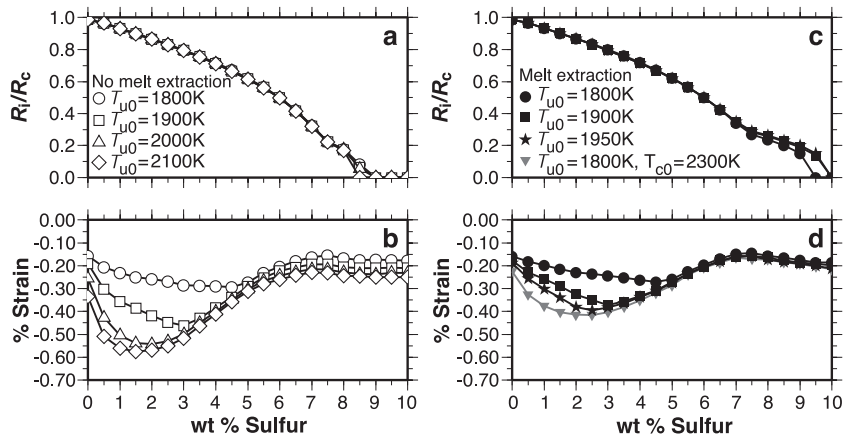


Fig. 5. Comparison of the effects of initial temperature on models without (a and b) and with (c and d) mantle melt extraction and crustal growth. Panels (a) and (c) show the normalized inner core radius, while panels (b) and (d) give the accumulated surface strain as functions of bulk core sulfur content for a dry-olivine mantle rheology and condensation-sequence-dominated U and Th.

sulfur contents less than 6 wt%, however, there is a marked increase in contractional strain with increasing initial temperature (Fig. 5b and d). The sulfur content beyond which the difference in time-integrated strain with increasing initial temperature is small is related to the melting point of Fe–FeS. Because of their relatively higher core melting temperatures, models with <6 wt% bulk core sulfur start with a solid inner core; an increase in initial temperature leads to a decrease in initial inner core size. Therefore, a larger fraction of the core solidifies over the last 4 Ga for initially warmer models, leading to larger integrated surface contraction. This point is further illustrated by the suite of models (inverted triangles in Fig. 5c and d) that have higher initial core temperatures.

There is an interesting trade-off in model cases that include melt production and growth of a crust (Fig. 5d). Increases in initial temperature lead to thicker crusts and larger fractions of heat-producing elements sequestered in the crust because of the increased depth extent of melting, melt fraction, and convective velocity (e.g., [24,29]). Instead of leading directly to an increase in predicted contractional strain with increased initial temperature at core sulfur contents greater than  $\sim 5$  wt% the predicted strains are similar in magnitude, independent of initial thermal condition, because of magmatically enhanced early cooling. Although larger initial temperatures result in more efficient extraction of heat

from the interior, the inner core begins to form at an earlier time and becomes larger at a given time than for counterpart models with lower initial temperatures (Fig. 5c). Comparatively more heat is therefore released via core differentiation and solidification, which offsets the effects of enhanced early cooling.

### 3.5. Effect of composition of heat-producing elements

The abundances of long-lived, heat-producing elements, both in absolute and relative terms, bear directly on the evolution of Mercury, in addition to potentially serving as a diagnostic indicator of the planet's formational process. Given the presently underconstrained nature of Mercury's heat-producing element composition (e.g., [34]), we test several possibilities for the composition of the silicate portion of the planet (Table 2). Formational models dominated by condensation processes tend to have enhanced amounts, relative to chondritic, of U and Th and lack K (e.g., [36]), while models dominated by a later volatilization of the silicate exterior suggest a Th-rich composition [37]. The 14-Gyr half-life of  $^{232}\text{Th}$  is sufficiently large relative to the half-lives of the radioactive isotopes of U and K that the rate of planetary cooling is lower, and hence over the last 4 Gyr less contraction would be expected for a planet with heat produced only by the decay of  $^{232}\text{Th}$  compared with one that contains significant U and possibly K. Alternatively,

given the observation of K in Mercury’s exosphere [38], we consider the model labeled “Condensation+K,” which has a composition similar to that suggested for the bulk composition of the Moon [50] and a heat productivity between that of the condensation and CI chondritic models (Fig. 6). We also examine the possibility that Mercury’s composition is related to that of CI chondrites (e.g., [35,51]), particularly a chondritic composition for the silicate layer or one-half as large resulting from impact stripping of a crust and upper mantle (e.g., [39]). The amount and time rate of decay of heat production for each of these models are quite different (Fig. 6). Results (Fig. 7) from models with the compositions in Table 2 bear out the prediction that a Th-dominated composition (i.e., from volatilization of an outer silicate shell) will have less integrated contractional surface strain than scenarios predicting significant U and K. At relatively high core sulfur contents, the Th-rich cases have noticeably smaller inner cores (or no inner core) than those with U and K as well as Th. At core sulfur contents  $>6.5$  wt%, the Th-rich models predict  $\sim 0.1\%$  contractional strain. For core sulfur contents  $>7.5$  wt%, no inner core forms to help drive convection in the outer core; a magnetic field driven at present by a core dynamo would therefore likely be precluded.

### 3.6. Effect of pressure on core melting relationships

A crucial component in modeling the evolution of planetary cores is knowledge of the melting relations

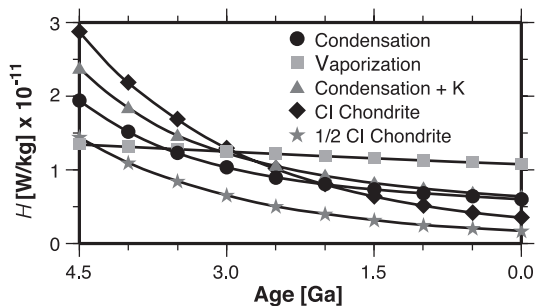


Fig. 6. Comparison of the amount of heat produced as a function of time for the heat-producing element compositions listed in Table 2.

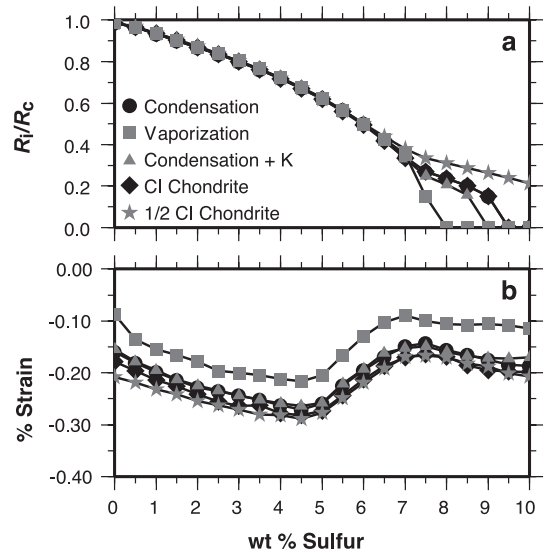


Fig. 7. Comparison of the effects of heat-producing element concentrations on (a) the normalized inner core radius and (b) the surface strain as functions of bulk core sulfur content for a dry-olivine mantle rheology, mantle melt extraction and crustal growth, and an initial upper mantle temperature of 1800 K.

of relevant materials. For the Fe–FeS system, laboratory experiments extend only to 25 GPa [26], yet Mercury’s central pressure is  $\sim 35$ –40 GPa. Because of limited data on the shape of the liquidus as a function of sulfur content, we utilize a linear approximation (e.g., [11,17]). The key parameter in this approximation is the nondimensional slope  $\alpha_c$  [17] of the liquidus, which connects the melting temperature for pure Fe with the melting temperature at the Fe–FeS eutectic composition at a given pressure. Recent laboratory data suggest that there is a linear increase in eutectic temperature with pressure at pressures  $>14$  GPa and that the eutectic composition is approximately constant above 20 GPa [21,26]. These data give  $\alpha_c = 2.4$  for conditions appropriate to the deep core of Mercury and  $\sim 3.3$  for conditions matching the shallow regions of the core. Results presented in Figs. 1–5 and 7 are based on the former value, but Fig. 8 illustrates the effect of the pressure dependence of the liquidus on predicted present inner-core radius and accumulated surface strain. Models with  $\alpha_c = 3.3$  have comparatively lower melting temperatures and yield smaller inner cores at present. The ranges of accumulated strains are similar for both values of  $\alpha_c$ , but the minimum contractional strain

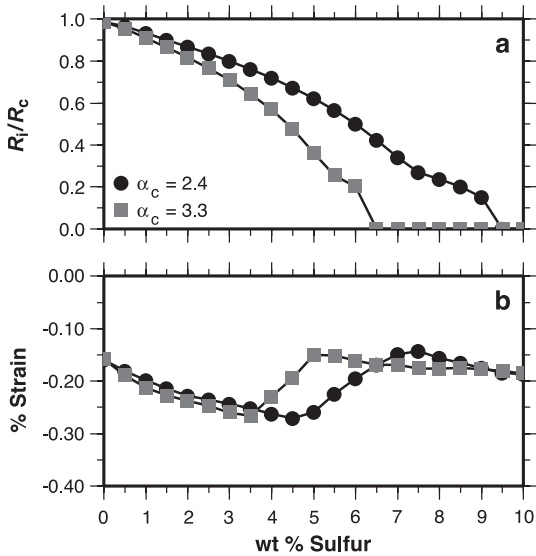


Fig. 8. Comparison of the effects of core liquidus slope,  $\alpha_c$ , extrapolated to conditions in the deep core vs. those in the shallow core on (a) the normalized inner core radius and (b) accumulated surface strain as functions of bulk core sulfur content for a dry-olivine mantle rheology, condensation-sequence-dominated U and Th, mantle melt extraction and crustal growth, and an initial upper mantle temperature of 1800 K.

occurs at approximately 2.5 wt% lower bulk core sulfur content for  $\alpha_c = 3.3$  than for  $\alpha_c = 2.4$ .

#### 4. Discussion

The tectonic record on Mercury's surface potentially provides an important constraint on the planet's interior evolution. Shortening inferred across individual lobate scarps together with the total length of scarps visible on the imaged portion of Mercury's surface indicate an average contractional strain of  $\sim 0.05$ – $0.1\%$  since the end of heavy bombardment [2,3]. At face value, this range in total strain strongly limits time-integrated internal cooling (e.g., absent an inner core,  $0.05\%$  strain is equivalent to 50 K of cooling since 4 Ga). If this constraint is to be met, the mantle must have cooled slowly over most of the planet's history. An accumulated contractional strain of no more than  $0.1\%$  would limit acceptable models to those with a dry-olivine mantle rheology, heat production provided by Th only (i.e., the composition suggested by late-stage silicate

vaporization [37]), and a bulk core sulfur content  $>6.5$  wt%.

The existence of an internal magnetic field on Mercury [7] may provide an additional constraint on the planet's internal evolution, but the nature of the constraint depends on the origin of the present field. A hydromagnetic-dynamo-generated magnetic field (e.g., [10,11]) requires a liquid and convecting outer core (e.g., [14]). Recent numerical dynamo simulations suggest that the character of the magnetic field and sustainability of a dynamo may depend on the fractional inner core radius ( $R_i/R_c$ ) [52–54]. A superadiabatic temperature gradient, which corresponds to a heat flux from the core of at least  $12$ – $13$   $\text{mW/m}^2$  (given a core thermal conductivity of  $\sim 40$   $\text{W/(m K)}$ ) [55] and the parameters in Table 1), or growth of an inner core with its attendant release of buoyant S, may independently be sufficient to drive outer core convection. Imposition of the constraint that heat loss, chemical buoyancy, or both drive outer core convection, together with the surface-strain constraint, further restricts acceptable models to  $6.5$ – $7.5$  wt% bulk core sulfur content and a silicate heat production provided only by the decay of Th. None of the models tested can satisfy both the surface-strain constraint and a requirement of a superadiabatic core heat flux, which would imply a thermal source for core convection that generates a modern dynamo. This point is illustrated by the fact that the only models tested that have a superadiabatic core heat flux at present (i.e., those with  $7.5$ – $8.5$  wt% bulk core S and a wet-olivine mantle rheology in Fig. 4) also have total contractional strains more than twice that inferred from lobate scarps. However, requiring a superadiabatic heat flux to drive a dynamo may be too restrictive because the energy released at the liquid–solid core interface to drive compositional convection needs only to exceed  $\sim \varepsilon Q_{\text{cond}}$ , where  $\varepsilon$  is a Carnot efficiency ( $\sim 0.1$ ) and  $Q_{\text{cond}}$  is the heat conducted along the adiabat (e.g., [17,56]), a condition met by models that have inner core growth. We note that the wet-olivine rheology models with  $7.5$ – $8.5$  wt% S in the core (Fig. 4) have a convecting mantle and those with  $9$ – $10$  wt% S have a conductive mantle at present. This difference is the result of smaller mantle Rayleigh numbers in the models with  $9$ – $10$  wt% S due to their thinner silicate shell, a consequence of their relatively less dense cores and

the fixed moment of inertia ( $C/MR^2=0.33$ ) adopted for all models.

Because the question of the origin of Mercury's magnetic field is open, the nature of the constraint that the field poses for the planet's evolution is uncertain. While crustal remanent magnetization has not been the preferred mechanism for field generation (e.g., [11]), a crustal source imposes the alternative constraint on Mercury's evolution that a core field likely was generated early in the planet's history because a substantial fraction of the crust on the hemisphere imaged by Mariner 10 predates the end of heavy impact bombardment. In order for the crust to acquire strong, coherent magnetization, a hydromagnetic dynamo is probably needed. Such a dynamo could be driven by early, rapid cooling of the core as it loses any initial superheat. Early, rapid heat loss by this mechanism is a general feature of all of our models (e.g., Fig. 1). Another alternative explanation for Mercury's modern field is a thermoelectric dynamo, which requires mantle convection, or at least recent cessation of mantle convection, in order to maintain temperature differences along the core–mantle boundary [57].

The range of compositional models tested (Table 2, Figs. 6, 7) was guided by proposed explanations for Mercury's large uncompressed density, including vaporization of the mantle in the early solar nebula [37], a condensation-sequence-dominated composition [36], or impact-stripping of the crust and upper mantle [39]. Models with significant U and K (i.e., condensation, condensation+K, CI chondrite, 1/2 CI chondrite) do not satisfy the stated constraints on Mercury's thermal evolution as well as those with Th (i.e., vaporization) as the primary internal heat source because of the longer half-life for  $^{232}\text{Th}$ .

There are reasons to treat the tectonic constraint on accumulated contractional strain, however, with some caution. Because less than half the planet's surface has been imaged, inferences of global contraction include an assumption that unimaged portions of the planet have experienced strain comparable to that in the imaged hemisphere. Furthermore, there may be other mechanisms for accommodating surface strain, such as long-wavelength, low-amplitude, lithospheric folding [6] or pervasive small-scale faulting unresolved in Mariner

10 images [2]. While such structures are not discernible in available data, the forthcoming MESSENGER mission promises topographic measurements and stereo imaging observations that will be sensitive to such features (e.g., [22]). Should the total accumulated global contraction be smaller than current estimates, then none of the models tested here may be acceptable. If, however, Mercury's surface hosts more contractional strain than has been inferred from the lobate scarps imaged by Mariner 10 [2,3], even by a factor of two, then the envelope of viable models opens to include all of the heat production compositions tested as long as the bulk core sulfur content is generally greater than about 6 wt%.

Modeled crustal production could be compared with estimates of Mercury's crustal thickness as an additional constraint [24]. However, the range of crustal thickness estimates is large (i.e., from  $\leq 140$  km [58] to 100–300 km [59]) as are the absolute values, and none of the models tested here produce crust as voluminous as the largest of these values. Neglecting the uncertainties in such determinations, either a peridotite-dominated mantle is inappropriate for Mercury or much of the crust is primordial, and our calculations represent a surface veneer of younger magmatic material as has been discussed for Mars [24]. If there were significant magmatic additions to the crust subsequent to the end of heavy bombardment, particularly if such melt were generated at depths within the stability field of garnet, the reduction in density of both the extracted and residuum components could partially offset the effects of global cooling on the surface strain field [60]. Substantial additions to the crust after heavy bombardment are not predicted by our models, however, and there is no evidence for such a crustal formation history from the Mariner 10 images (e.g., [61]).

An important unresolved issue is the timing of lobate scarp formation. If net cooling of the planet is the mechanism responsible, then contraction should have been gradual and lobate scarp formation continuous. A source of uncertainty is the time that strain accumulation in our models should begin; we calculate that a 100 My change in  $t_e$  results in at most a 0.02% strain offset (e.g.,  $t_e=3.9$  Ga has 0.02% less strain than the same model with  $t_e=4.0$  Ga). The

result is likely less significant than the uncertainty in the actual contractional strain estimates. Lobate scarps are generally inferred to postdate the intercrater plains on the grounds that no scarp is seen to be embayed by such plain material (e.g., [62,63]). Scarps deform a number of large impact craters on Mercury, and scarps are seen on the smooth plains, the youngest geological unit [2,61,62,64]. All of these observations are consistent with scarp formation onset near the end of heavy bombardment and a continuation of contraction until sometime after smooth plains emplacement. That the largest and best-developed scarps deform older units suggests that the rate of planetary contraction slowed considerably near the end of heavy bombardment. Such a temporal change is broadly consistent with a transition from a convecting to a conductive mantle as is predicted by most of our models.

## 5. Summary

We have explored models for the coupled thermal, magmatic, and tectonic history of Mercury to investigate the conditions under which current inferences of planetary contraction and a dynamo origin for the planet's present internal magnetic field can both be satisfied. In general, our results suggest that these limited constraints can be best met by a model with a dry-olivine rheology, a bulk core sulfur content of 6.5–7.5 wt%, and heat production dominated by the decay of  $^{232}\text{Th}$ , as predicted by the vaporization model for the origin of Mercury's high metal/silicate ratio [37]. Presently accepted values for the accumulated contraction of Mercury are neither upper nor lower bounds, however, because the portion of the planet not seen by Mariner 10 may display more or less shortening accommodated in large, surface-breaking, thrust faults. Furthermore, long-wavelength, low-amplitude folding [6] or possibly a weak surface layer [65] with pervasive small-scale faulting may accommodate additional strain. A larger value for accumulated contraction would permit some combination of a smaller sulfur fraction in the core, a modest amount of water in the mantle, or a significant K content in the crust and mantle.

Future observations of the planet by spacecraft, including the MESSENGER and BepiColombo mis-

sions, will yield key information on Mercury's internal structure and evolution. Measurement of the moment of inertia and the amplitude of the physical libration of the planet will constrain the state and size of the core (e.g., [66]). High-resolution topographic measurements may resolve whether long-wavelength folding has accommodated contractional strain and will aid in the quantification of shortening across lobate scarps and other tectonic features. Measurement of Mercury's surface composition, including the abundances of U, Th, and K, will constrain internal heat production and thermal evolution models as well as potentially distinguish among hypotheses for the planet's formation. Observations of the geometry of Mercury's magnetic field should distinguish crustal remanence from core dynamo models. These future observations will substantially advance our understanding of the geological and geophysical evolution of the innermost terrestrial planet.

## Acknowledgements

We thank Jon Aurnou for discussions on the operation of a core dynamo. Comments from Francis Nimmo and two anonymous reviewers helped sharpen the manuscript. This work was supported by the NASA Planetary Geology and Geophysics Program under grants NAG5-10165 and NAG5-4448. *[SK]*

## Appendix A

To calculate the evolution of surface strain on Mercury, we represent the lithosphere as a thick, elastic, spherical shell overlying an inviscid fluid interior. This one-dimensional representation, modified from [67], differs from earlier thin-shell models of lithospheres (e.g., [45]). Material properties of the shell are taken to be constant, although temperature can vary radially. By symmetry, there are three non-zero components of the stress tensor, only two of which are independent:  $\sigma_{rr}$  is the radial component, and  $\sigma_{\theta\theta} = \sigma_{\phi\phi}$  is the tangential component. We start with the equation of equilibrium:

$$\frac{d\sigma_{rr}}{dr} + \frac{2}{r}(\sigma_{rr} - \sigma_{\theta\theta}) = 0. \quad (\text{A1})$$

The stress and strain relationships, under linear elasticity, are given by

$$\varepsilon_{rr} - \alpha_l(T_b - T) = \frac{1}{E}(\sigma_{rr} - 2\nu\sigma_{\theta\theta}) \quad (\text{A2a})$$

$$\varepsilon_{\theta\theta} - \alpha_l(T_b - T) = \frac{1}{E}[\sigma_{\theta\theta} - \nu(\sigma_{rr} + \sigma_{\theta\theta})], \quad (\text{A2b})$$

where  $\alpha_l$  is the linear coefficient of thermal expansion,  $E$  is the Young's modulus,  $\nu$  is Poisson's ratio,  $T$  is temperature, and  $T_b$  is the elastic blocking temperature (e.g., [45]), the temperature above which elastic stresses are not supported. For a radial displacement,  $u$ , the radial and tangential strains are

$$\varepsilon_{rr} = \frac{\partial u}{\partial r} \quad (\text{A3a})$$

$$\varepsilon_{\theta\theta} = \frac{u}{r}. \quad (\text{A3b})$$

By rearranging Eqs. (A2a) (A2b), we can solve for the radial and tangential stress components:

$$\sigma_{rr} = \frac{E}{(1+\nu)(1-2\nu)} [(1-\nu)\varepsilon_{rr} + 2\nu\varepsilon_{\theta\theta} - (1+\nu)\alpha_l(T_b - T)] \quad (\text{A4a})$$

$$\sigma_{\theta\theta} = \frac{E}{(1+\nu)(1-2\nu)} [\varepsilon_{\theta\theta} + \nu\varepsilon_{rr} - (1+\nu)\alpha_l(T_b - T)]. \quad (\text{A4b})$$

Then substituting Eqs. (A3a,b) and (A4a,b) into Eq. (A1), we obtain

$$\frac{\partial}{\partial r} \left[ \frac{1}{r^2} \frac{\partial}{\partial r} (r^2 u) \right] = \left( \frac{1+\nu}{1-\nu} \right) \frac{\partial}{\partial r} [\alpha_l(T_b - T)]. \quad (\text{A5})$$

Integrating twice and rearranging terms, it can be shown that the displacement within the lithosphere satisfies

$$u(r) = \left( \frac{1+\nu}{1-\nu} \right) \frac{\alpha_l}{r^2} \int_a^r [T_b - T(s)] s^2 ds + C_1 r + C_2 \frac{1}{r^2}, \quad (\text{A6})$$

where  $s$  is a dummy variable of integration,  $C_1$  and  $C_2$  are unknown constants of integration, and  $a$  is the base of the elastic lithosphere, defined by  $T_b$ . To evaluate Eq. (A3a), we multiply Eq. (A6) by  $r^2$  and then differentiate with respect to  $r$ :

$$\frac{\partial u(r)}{\partial r} = \left( \frac{1+\nu}{1-\nu} \right) \alpha_l [T_b - T(r)] + 3C_1 - \frac{2}{r} u(r). \quad (\text{A7})$$

To find the constants,  $C_1$  and  $C_2$ , we apply boundary conditions at the top and bottom surfaces of the elastic shell. Then, using (Eqs. (A3a,b), (A4a), (A6), (A7)), and because there is no load at the surface ( $r=b$ )  $\sigma_{rr}(b)=0$ , so at  $r=b$ :

$$-\frac{2E}{(1-\nu)} \frac{\alpha_l}{b^3} \int_a^b [T_b - T(s)] s^2 ds + C_1 \frac{E}{1-2\nu} - C_2 \frac{2E}{(1+\nu)} \frac{1}{b^3} = 0. \quad (\text{A8})$$

For convenience, we define

$$\chi \equiv -\frac{2E}{(1-\nu)} \frac{\alpha_l}{b^3} \int_a^b [T_b - T(s)] s^2 ds \quad (\text{A9})$$

so that Eq. (A8) simplifies to

$$C_2 = \frac{(1+\nu)b^3}{2E} \left[ \frac{C_1 E}{1-2\nu} + \chi \right]. \quad (\text{A10})$$

At the base of the elastic shell ( $r=a$ ),  $T_b = T(a)$  and

$$\varepsilon_{\theta\theta}(a) = \frac{1}{E} [(1-\nu)\sigma_{\theta\theta}(a) - \nu\sigma_{rr}(a)]. \quad (\text{A11})$$

Using Eqs. (A3a,b) and (A6), (A7) to expand Eqs. (A4a,b), we have

$$\sigma_{rr}(a) = C_1 \frac{E}{(1-2\nu)} - C_2 \frac{2E}{(1+\nu)} \frac{1}{a^3} \quad (\text{A12a})$$

$$\sigma_{\theta\theta}(a) = C_1 \frac{E}{(1-2\nu)} + C_2 \frac{E}{(1+\nu)} \frac{1}{a^3}. \quad (\text{A12b})$$

Substituting Eqs. (A12a,b) into Eq. (A11) and simplifying, we obtain the following expression for horizontal strain at the base of the elastic shell:

$$\varepsilon_{\theta\theta}^e(a) = C_1 + \frac{1}{a^3} C_2. \quad (\text{A13})$$

Vertical displacements [and  $\varepsilon_{\theta\theta}$  by Eq. (A3b)] across the fluid–solid interface must be continuous, so  $\varepsilon_{\theta\theta}^f = \varepsilon_{\theta\theta}^s$ . The strain at the top of the fluid interior is directly related to the volume change of the interior:

$$\varepsilon_{\theta\theta}^f(a) = \frac{1}{3}\alpha_{v,i}\delta\bar{T}_i + \frac{1}{3}\bar{\beta}\delta\sigma_{rr}(a) - \frac{1}{3}f_{ic}\xi, \quad (\text{A14})$$

where  $\alpha_v$  is the volumetric coefficient of thermal expansion ( $\alpha_v = 3\alpha_l$ ),  $\delta\bar{T}$  is an appropriately averaged internal temperature change,  $\bar{\beta}$  is the appropriately averaged compressibility,  $\delta\sigma_{rr}$  is the change in volumetric stress,  $f_{ic}$  is the fraction of the interior represented by the solid inner core, and  $\xi$  is the fractional volume change of iron upon solidification (e.g., [4]). Formally,  $\alpha_{v,i}\delta\bar{T}$  and  $\bar{\beta}$  are

$$\alpha_{v,i}\delta\bar{T}_i = f_m\alpha_{v,m}\delta\bar{T}_m + f_{oc}\alpha_{v,oc}\delta\bar{T}_{oc} + f_{ic}\alpha_{v,ic}\delta\bar{T}_{ic} \quad (\text{A15a})$$

$$\bar{\beta} = f_m\beta_m + f_{oc}\beta_{oc} + f_{ic}\beta_{ic}, \quad (\text{A15b})$$

where  $f$  denotes volume fraction and the subscripts m, oc, and ic represent mantle, outer core, and inner core contributions, respectively. Substituting Eq. (A12a) into Eq. (A14) and combining with Eq. (A13) gives

$$\left[1 - \frac{\bar{\beta}E}{3(1-2\nu)}\right]C_1 + \left[1 + \frac{2\bar{\beta}E}{3(1+\nu)}\right] \times \frac{1}{a^3}C_2 = \frac{1}{3}\alpha_v\delta\bar{T}_i - \frac{1}{3}f_{ic}\xi, \quad (\text{A16})$$

and substituting in Eq. (A10) gives in terms of  $C_1$  only:

$$Z_1C_1 + Z_2\frac{1}{a^3}Z_3[Z_4C_1 + \chi] = \frac{1}{3}\alpha_v\delta\bar{T}_i - \frac{1}{3}f_{ic}\xi, \quad (\text{A17})$$

where

$$Z_1 = 1 - \frac{\bar{\beta}E}{3(1-2\nu)}, \quad Z_2 = 1 + \frac{2\bar{\beta}E}{3(1+\nu)}, \\ Z_3 = \frac{(1+\nu)b^3}{2E}, \quad Z_4 = \frac{E}{1-2\nu}. \quad (\text{A18})$$

Combining Eq. (A10) with Eqs. (A16) (A17) (A18) and substituting into Eq. (A6) completes the solution for  $u$  and, with Eqs. (A7) and (A3a,b), the thermo-elastic strains.

The corresponding strain rates are:

$$\dot{\varepsilon}_{rr} = \frac{\partial \dot{u}}{\partial r} \quad (\text{A19a})$$

$$\dot{\varepsilon}_{\theta\theta} = \frac{\dot{u}}{r}. \quad (\text{A19b})$$

Taking the first time derivative of Eqs. (A6) and (A7) gives

$$\dot{u}(r) = -\frac{(1+\nu)}{(1-\nu)}\frac{\alpha_l}{r^2}\int_a^r \dot{T}(s)s^2 ds + \dot{C}_1 r + \dot{C}_2 \frac{1}{r^2} \quad (\text{A20})$$

$$\frac{\partial \dot{u}(r)}{\partial r} = -\frac{(1+\nu)}{(1-\nu)}\alpha_l[\dot{T}(r)] + 3\dot{C}_1 - \frac{2}{r}\dot{u}(r). \quad (\text{A21})$$

$\dot{T}$  and  $\dot{a}$  (the time rate of change of the depth of the base of the elastic lithosphere, which is used below) are found directly from the thermal solution (i.e., [24]). In order to find  $\dot{C}_2$ , we start with Eq. (A10) and differentiate with respect to time to obtain

$$\dot{C}_2 = \frac{(1+\nu)b^3}{2E}\left[\frac{\dot{C}_1 E}{1-2\nu} + \dot{\chi}\right], \quad (\text{A22})$$

where  $\dot{\chi}$  is given by

$$\dot{\chi} = \frac{2E}{1-\nu}\frac{\alpha_l}{b^3}\int_a^b \dot{T}(s)s^2 ds. \quad (\text{A23})$$

Then, by rearranging Eqs. (A17), (A18) and differentiating with respect to time, we have

$$\dot{C}_1[a^3Z_1 + Z_2Z_3Z_4] + C_1[3a^2Z_1]\dot{a} = \frac{1}{3}\alpha_v[3a^2\delta T_c\dot{a} + a^3\delta\dot{T}_c] - Z_2Z_3\dot{\chi} - \frac{1}{3}\xi[3a^2f_{ic}\dot{a} + a^3\dot{f}_{ic}]. \quad (\text{A24})$$

Combining Eqs. (A20) (A21) (A22) and (A24) into Eqs. (A19a,b) completes the solution for strain rates.

## References

- [1] B.C. Murray, The Mariner 10 pictures of Mercury: an overview, *J. Geophys. Res.* 80 (1975) 2342–2344.
- [2] R.G. Strom, N.J. Trask, J.E. Guest, Tectonism and volcanism on Mercury, *J. Geophys. Res.* 80 (1975) 2478–2507.
- [3] T.R. Watters, M.S. Robinson, A.C. Cook, Topography of lo-

- bate scarps on Mercury: new constraints on the planet's contraction, *Geology* 26 (1998) 991–994.
- [4] S.C. Solomon, Some aspects of core formation in Mercury, *Icarus* 28 (1976) 509–521.
- [5] B.C. Murray, M.J.S. Belton, G.E. Danielson, M.E. Davies, D.E. Gault, B. Hapke, B. O'Leary, R.G. Strom, V. Suomi, N. Trask, Mercury's surface: preliminary description and interpretation from Mariner 10 pictures, *Science* 185 (1974) 169–179.
- [6] A.J. Dombard, S.A. Hauck II, S.C. Solomon, R.J. Phillips, Potential for long-wavelength folding on Mercury, *Lunar Planet. Sci.* 32 (abstract 2035 CD-ROM).
- [7] N.F. Ness, K.W. Behannon, R.P. Lepping, Y.C. Whang, The magnetic field of Mercury. I, *J. Geophys. Res.* 80 (1975) 2708–2716.
- [8] L.J. Srnka, Magnetic dipole moment of a spherical shell with TRM acquired in a field of internal origin, *Phys. Earth Planet. Inter.* 11 (1976) 184–190.
- [9] A. Stephenson, Crustal remanence and the magnetic moment of Mercury, *Earth Planet. Sci. Lett.* 28 (1976) 454–458.
- [10] J.E.P. Connerney, N.F. Ness, Mercury's magnetic field and interior, in: F. Vilas, C.R. Chapman, M.S. Matthews (Eds.), *Mercury*, University of Arizona Press, Tucson, 1988, pp. 494–513.
- [11] G. Schubert, M.N. Ross, D.J. Stevenson, T. Spohn, Mercury's thermal history and the generation of its magnetic field, in: F. Vilas, C.R. Chapman, M.S. Matthews (Eds.), *Mercury*, University of Arizona Press, Tucson, 1988, pp. 429–460.
- [12] M.H. Acuña, J.E.P. Connerney, N.F. Ness, R.P. Lin, D. Mitchell, C.W. Carlson, J. McFadden, K.A. Anderson, H. Reme, C. Mazelle, D. Vignes, P. Wasilewski, P. Cloutier, Global distribution of crustal magnetization discovered by the Mars Global Surveyor MAG/ER experiment, *Science* 284 (1999) 790–798.
- [13] O. Aharonson, M.T. Zuber, S.C. Solomon, Crustal remanence in an internally magnetized non-uniform shell: a possible source for Mercury's magnetic field? *Earth Planet. Sci. Lett.* 218 (2004) 261–268.
- [14] R.T. Merrill, M.W. McElhinny, P.L. McFadden, *The Magnetic Field of the Earth*, Academic Press, New York, 1998, 531 pp.
- [15] V.R. Murthy, H.T. Hall, The chemical composition of the Earth's core: possibility of sulphur in the core, *Phys. Earth Planet. Inter.* 2 (1970) 276–282.
- [16] R.W. Siegfried II, S.C. Solomon, Mercury: internal structure and thermal evolution, *Icarus* 23 (1974) 192–205.
- [17] D.J. Stevenson, T. Spohn, G. Schubert, Magnetism and thermal evolution of the terrestrial planets, *Icarus* 54 (1983) 466–489.
- [18] V.S. Solomatov, L.-N. Moresi, Scaling of time-dependent stagnant lid convection: application to small-scale convection on Earth and other terrestrial planets, *J. Geophys. Res.* 105 (2000) 21795–21817.
- [19] G. Schubert, D.L. Turcotte, P. Olson, *Mantle Convection in the Earth and Planets*, Cambridge Univ. Press, Cambridge, UK, 2001, 940 pp.
- [20] R. Boehler, Melting of the Fe–FeO and the Fe–FeS systems at high pressure: constraints on core temperatures, *Earth Planet. Sci. Lett.* 111 (1992) 217–227.
- [21] Y. Fei, C.M. Bertka, L.W. Finger, High-pressure iron sulfur compound, Fe<sub>3</sub>S<sub>2</sub>, and melting relations in the Fe–FeS system, *Science* 275 (1997) 1621–1623.
- [22] S.C. Solomon, R.L. McNutt Jr., R.E. Gold, M.H. Acuña, D.N. Baker, W.V. Boynton, C.R. Chapman, A.F. Cheng, G. Gloeckler, J.W. Head III, S.M. Krimigis, W.E. McClintock, S.L. Murchie, S.J. Peale, R.J. Phillips, M.S. Robinson, J.A. Slavin, D.E. Smith, R.G. Strom, J.I. Trombka, M.T. Zuber, The MESSENGER mission to Mercury: scientific objectives and implementation, *Planet. Space Sci.* 49 (2001) 1445–1465.
- [23] R. Grard, A. Balogh, Returns to Mercury: science and mission objectives, *Planet. Space Sci.* 49 (2001) 1395–1407.
- [24] S.A. Hauck II, R.J. Phillips, Thermal and crustal evolution of Mars, *J. Geophys. Res.* 107 (2002) 5052 (doi:10.1029/2001JE001801).
- [25] T. Kleine, C. Münker, K. Mezger, H. Palme, Rapid accretion and early core formation on asteroids and the terrestrial planets from Hf–W chronometry, *Nature* 418 (2002) 952–955.
- [26] Y. Fei, J. Li, C.M. Bertka, C.T. Prewitt, Structure type and bulk modulus of Fe<sub>3</sub>S, a new iron–sulfur compound, *Am. Mineral.* 85 (2000) 1830–1833.
- [27] O.L. Anderson, The three-dimensional phase diagram of iron, in: V. Dehant, K.C. Creager, S.-I. Karato, S. Zatman (Eds.), *Earth's Core: Dynamics, Structure, Rotation*, American Geophysical Union, Washington, DC, 2003, pp. 83–103.
- [28] H. Harder, G. Schubert, Sulfur in Mercury's core? *Icarus* 151 (2001) 118–122.
- [29] D.P. McKenzie, M.J. Bickle, The volume and composition of melt generated by extension of the lithosphere, *J. Petrol.* 29 (1988) 625–679.
- [30] J. Zhang, C.T. Herzberg, Melting experiments on anhydrous peridotite KLB-1 from 5.0 to 22.5 GPa, *J. Geophys. Res.* 99 (1994) 17729–17742.
- [31] O. Grasset, E.M. Parmentier, Thermal convection in a volumetrically heated, infinite Prandtl number fluid with strongly temperature-dependent viscosity: implications for planetary thermal evolution, *J. Geophys. Res.* 103 (1998) 18171–18181.
- [32] C.C. Reese, V.S. Solomatov, L.N. Moresi, Non-Newtonian stagnant lid convection and magmatic resurfacing on Venus, *Icarus* 139 (1999) 67–80.
- [33] C. Dumoulin, M.-P. Doin, L. Fleitout, Heat transport in stagnant lid convection with temperature- and pressure-dependent Newtonian or non-Newtonian rheology, *J. Geophys. Res.* 104 (1999) 12759–12777.
- [34] K.A. Goettel, Present bounds on the bulk composition of Mercury: implications for planetary formation processes, in: F. Vilas, C.R. Chapman, M.S. Matthews (Eds.), *Mercury*, University of Arizona Press, Tucson, 1988, pp. 613–621.
- [35] K. Lodders, B. Fegley Jr., *The Planetary Scientist's Companion*, Oxford Univ. Press, New York, NY, 1998, 371 pp.
- [36] Basaltic Volcanism Study Project, *Basaltic Volcanism on the Terrestrial Planets*, Pergamon, New York, 1981, 1286 pp.
- [37] B. Fegley Jr., A.G.W. Cameron, A vaporization model for iron/silicate fractionation in the Mercury protoplanet, *Earth Planet. Sci. Lett.* 82 (1987) 207–222.
- [38] A.E. Potter, T.H. Morgan, Potassium in the atmosphere of Mercury, *Icarus* 67 (1986) 336–340.
- [39] A.G.W. Cameron, B. Fegley Jr., W. Benz, W.L. Slattery, The

- strange density of Mercury: theoretical considerations, in: F. Vilas, C.R. Chapman, M.S. Matthews (Eds.), *Mercury*, University of Arizona Press, Tucson, 1988, pp. 692–708.
- [40] S.-I. Karato, P. Wu, Rheology of the upper mantle: a synthesis, *Science* 260 (1993) 771–778.
- [41] R. Jeanloz, D.L. Mitchell, A.L. Sprague, I. de Pater, Evidence for a basalt-free surface on Mercury and implications for internal heat, *Science* 268 (1995) 1455–1457.
- [42] M.S. Robinson, G.J. Taylor, Ferrous oxide in Mercury's crust and mantle, *Meteorit. Planet. Sci.* 36 (2001) 841–847.
- [43] M.M. Hirschmann, Mantle solidus: experimental constraints and the effects of peridotite composition, *Geophys. Geochem. Geosyst.* 1 (doi:10.1029/2000GC000070).
- [44] C.T. Herzberg, P. Ratteron, J. Zhang, New experimental observations on the anhydrous solidus for peridotite KLB-1, *Geophys. Geochem. Geosyst.* 1 (doi:10.1029/2000GC000089).
- [45] D.L. Turcotte, Thermal stresses in planetary elastic lithospheres, *J. Geophys. Res.* 88 (1983) A585–A587.
- [46] M.K. McNutt, Lithospheric flexure and thermal anomalies, *J. Geophys. Res.* 89 (1984) 11180–11194.
- [47] D.A. Wiens, S. Stein, Age dependence of oceanic intraplate seismicity and implications for lithospheric evolution, *J. Geophys. Res.* 88 (1983) 6455–6468.
- [48] S.-I. Karato, M.S. Paterson, J.D. Fitzgerald, Rheology of synthetic olivine aggregates—influence of grain size and water, *J. Geophys. Res.* 91 (1986) 8151–8176.
- [49] S. Mei, D.L. Kohlstedt, Influence of water on plastic deformation of olivine aggregates: 2. Dislocation creep regime, *J. Geophys. Res.* 105 (2000) 21471–21481.
- [50] S.R. Taylor, Lunar and terrestrial crusts—a contrast in origin and evolution, *Phys. Earth Planet. Inter.* 29 (1982) 233–241.
- [51] W.F. McDonough, S.S. Sun, The composition of the Earth, *Chem. Geol.* 120 (1995) 223–253.
- [52] D. Jault, Magnetic field generation impeded by inner cores of planets, *C. R. Acad. Sci., II A* 323 (1996) 451–458.
- [53] J.M. Aurnou, F. Al-Shamali, M. Heimpel, Dynamo processes in a thin shell geometry, *Eos Trans. AGU* 82 (Fall Meet. Suppl., abstract GP31-0176).
- [54] S. Stanley, J. Bloxham, W.E. Hutchison, M.T. Zuber, Can Mercury's weak surface magnetic field be generated by a dynamo? *Eos Trans. AGU* 84 (Fall Meet. Suppl., abstract P31-04).
- [55] F.D. Stacey, O.L. Anderson, Electrical and thermal conductivities of Fe–Ni–Si alloy under core conditions, *Phys. Earth Planet. Inter.* 124 (2001) 153–162.
- [56] D. Gubbins, Energetics of the Earth's core, *J. Geophys.* 43 (1977) 453–464.
- [57] D.J. Stevenson, Mercury's magnetic field: a thermoelectric dynamo? *Earth Planet. Sci. Lett.* 82 (1987) 114–120.
- [58] F. Nimmo, T.R. Watters, Depth of faulting on Mercury: implications for heat flux and crustal and effective elastic thickness, *Geophys. Res. Lett.* 31 (2004) L02701 (doi:10.1029/2003GL018847).
- [59] J.D. Anderson, R.F. Jurgens, E.L. Lau, M.A. Slade III, G. Schubert, Shape and orientation of Mercury from radar ranging data, *Icarus* 124 (1996) 690–697.
- [60] R.L. Kirk, D.J. Stevenson, The competition between thermal contraction and differentiation in the stress history of the Moon, *J. Geophys. Res.* 94 (1989) 12133–12144.
- [61] P.D. Spudis, J.E. Guest, Stratigraphy and geologic history of Mercury, in: F. Vilas, C.R. Chapman, M.S. Matthews (Eds.), *Mercury*, University of Arizona Press, Tucson, 1988, pp. 118–164.
- [62] B.M. Cordell, Tectonism and the interior of Mercury, PhD thesis, University of Arizona, 1977, 124 pp.
- [63] R.G. Strom, Mercury—an overview, *Adv. Space Res.* 19 (1997) 1471–1485.
- [64] B.M. Cordell, R.G. Strom, Global tectonics of mercury and the moon, *Phys. Earth Planet. Inter.* 15 (1977) 146–155.
- [65] M.E. Pritchard, D.J. Stevenson, Thermal aspects of a lunar origin by giant impact, in: R.M. Canup, K. Righter (Eds.), *Origin of the Earth and Moon*, University of Arizona Press, Tucson, 2000, pp. 179–196.
- [66] S.J. Peale, R.J. Phillips, S.C. Solomon, D.E. Smith, M.T. Zuber, A procedure for determining the nature of Mercury's core, *Meteorit. Planet. Sci.* 37 (2002) 1269–1283.
- [67] S. Timoshenko, J.N. Goodier, *Theory of Elasticity*, McGraw-Hill, New York, 1951, 506 pp.